Kovove Mater. 49 2011 233–242
DOI: 10.4149/km_2011_3_233

Nanoindentation applied to an optimized FSW-AZ31 butt joint

M. Cabibbo[1]*, P. Ricci[1], M. Regev[2]

[1] *Dipartimento di Meccanica, Università Politecnica delle Marche, 60131-Ancona, Italy*
[2] *Mechanical Engineering Department, Ort Braude College of Engineering, P.O. Box 78, Karmiel 21982, Israel*

Received 28 October 2010, received in revised form 10 February 2011, accepted 10 March 2011

Abstract

Friction stir welding (FSW) technique was used to weld AZ31B-H24 alloy plates. The effect of the welding parameters, probe traverse velocity and probe revolution rate, on the butt joint quality was investigated. A sound FSW AZ31 butt joint was produced with a revolution rate to probe traverse ratio ω/υ of 100 rev mm^{-1}. Equiaxed grains were observed at the weld nugget zone and in the base metal. Larger grains were detected in the nugget compared to the base metal. Hardness measurements were performed using nanoindentation techniques. Nanohardness was compared to the more conventional microhardness measurements both performed along the mid-thickness of the cross section and along upper and lower surfaces. Nanohardness at the weld nugget zone was quite similar to that of the base metal, while a significant peak was detected at the TMAZ/HAZ interface. This peak was higher at the advancing side of the FSW joint than the one observed at the retreating side.

K e y w o r d s: magnesium alloys, nanoindentation, friction stir welding

1. Introduction

In the last three decades, the growing demand for better fuel economy, reduction of exhaust gas emission and higher efficiency in transportation applications has promoted an extensive research into light-weight structural materials. Magnesium alloys are the lightest structural materials in industrial applications [1]. They have low density, high specific strength, high specific stiffness and excellent machinability. For these reasons, magnesium alloys are widely used in aerospace, automotive, and electronics industry [2, 3]. Due to the limited number of slip systems available in the hexagonal structure at room temperature, magnesium alloys have limited workability at room temperature, but they have good formability at high temperature. On the other hand, the grain size strengthening efficiency in Mg alloys is higher than the one achievable in aluminium and other light-weight alloys [4]. Magnesium alloys are also attractive due to their electromagnetic interference shielding properties [2] and their recycling capability.

However, magnesium alloys suffer from poor weldability, chiefly because of their exceptional reaction tendency with oxygen and the other environmental gases. With their increasing application, a reliable joining process is required, but welding magnesium alloys still faces many challenges. They can be joined using a wide variety of processes, but conventional processes have exhibited some disadvantages such as porosity, evaporative loss of the alloying elements, high residual stresses, pores, slag, splash, and other defects in the fuse zone [5].

Friction stir welding (FSW) does constitute an alternative method to the more conventional fusion welding techniques, which can overcome the above mentioned disadvantages. FSW is a solid connection method invented and patented by the Welding Institute, UK, in 1991 [6]. Compared with the traditional fusion welding techniques, FSW exhibits many advantages, such as no splash, no smoke, and no oxidation, and it does not need a wire or a protective gas [7–9].

The key advantage of FSW over conventional fusion welding techniques is that a metallic bond is achieved below the melting point of the base material thus avoiding many of the metallurgical problems associated with the solidification process [10–12]. There-

*Corresponding author: tel.: +390712204728; fax: +390712204801; e-mail address: m.cabibbo@univpm.it

fore, the innovative FSW technique is quite promising processing method for broadening the industrial application of magnesium alloys. Indeed, the first studies in this field have shown that the joint efficiency of magnesium friction stir welds is typically very high [10–15]. Various studies have recently been reported on the FSW of Mg alloys and the topics covered can be classified into three areas: (i) microstructure and hardness, (ii) texture and fracture, and (iii) surface modification in metals and composites [16–22]. AZ (Mg-Al-Zn) and AM (Mg-Al-Mn) series of magnesium alloys show sound FSW joints with good properties and uniform microstructure by optimizing the FSW parameters [23–26]. A number of investigations have shown that under the influence of the FSW tool (i.e. mechanical deformation) and processing temperatures a fine recrystallized microstructure is formed at the weld nugget zone [12]. It has also been reported that the high dislocation density in the weld region further contributes to a more homogeneous hardness profile in the FSW Mg alloys [19].

The basic concept of FSW is remarkably simple. A rotating tool typically consisting of a massive cylindrical shoulder and a smaller profiled probe is plunged into the joint line between two butted plates and is then traversed along the butt line. As a solid state process, solidification problems associated with conventional fusion welding are avoided (or diminished). The tool is rotated and plunged into the joint line so that the shoulder makes an intimate contact with the workpiece surface and the probe is buried within the entire thickness of the workpieces. Friction between the tool and the workpiece generates heat, causing a plasticized zone to form under the tool shoulder and around the probe. The rotating tool is then traversed along the joint line, whereby the probe stirs the locally plasticized material forcing it to flow in the direction of tool revolution to be deposited behind the probe where it cools and consolidates.

Welding parameters, tool geometry, and joint design have significant effect on the material flow pattern and temperature distribution, thereby influencing the microstructure evolution of material. The tool geometry plays a critical role in material flow and in turn governs the traverse rate at which FSW can be conducted. The tool is responsible for the localized heating and for the material flow [8, 16, 26]. In the initial stage of tool plunge, the heating primarily results from the friction between probe and workpiece. Some additional heating results from the deformation of material. The friction between the shoulder and workpiece is the largest source of heating. The shoulder confines the heated volume of material. The second role of the tool is to stir and move the material.

This work presents a nanohardness characterization of an optimized FSW AZ31 alloy butt joint. A direct comparison between the more common microhardness and the nanohardness results was carried out. Nanohardness has been measured by using a nanoindenter. Continuously recording indentation techniques, such as nanoindentation, have become rapidly established as a means of determining the nano-scale mechanical properties of metallic materials because of their high resolutions in load, position, and displacement [27, 28]. One of the key advantages of this technique is that many mechanical properties, namely nanohardness and reduced Young's modulus, can be directly determined by the analyses of the indentation load-displacement data, and thus avoiding the need to image the hardness impression. This, in turn, facilitates the mechanical properties measurement on the submicron scale.

2. Experimental procedures and method

The material used in this study was a commercial AZ31B-H24 magnesium alloy, with a nominal chemical composition of Mg-3.0Al-1.0Zn (wt.%), in the form of 200 × 100 mm^2 plates, 3.175 mm thick. The above plates were butt welded using a VA65II SEIKI® CNC milling machine. A H-13 steel FSW tool was used, the tool consisted in a probe having a diameter of 4.5 mm, 3 mm height and a 20 mm diameter shoulder. The principal directions of the FSW geometry are denoted as welding direction (WD), transverse direction (TD) and normal direction (ND) (Fig. 1). The tool advancing side is defined as the side of the tool where the tangent direction of the tool revolution is the same as that of the welding, while the tool retreating side is the opposite. The welding optimization was achieved through different experimental conditions, which are listed in Table 1.

All the welded specimens were examined by low-magnification optical microscopy (macroscopic inspections). The welds showing the highest quality, according to their metallographic cross section inspections, were then radiographically checked.

Specimens for the microstructure inspections were ground, mechanically polished with an 0.25 μm diamond paste and then chemically etched using a solution of 4.5 g picric acid in 10 ml acetic, 70 ml ethanol, and 20 ml distilled water at room temperature. Optical micrographs were taken in a Leika® microscope and an image pro plus® software was used for the grain size evaluation. A linear intercept method was used for the evaluation of the mean grain size in the different FSW regions. Microstructure characterization and microhardness measurements were performed at the cross section (ND-TD, plane), and along the upper and lower surfaces (WD-TD, plane) of the FSW plates (Fig. 1b).

Microhardness measurements were taken using a REMET HX-1000® with a load of 200 gf and 15 s

Table 1. FSW experimental conditions for the optimization of the FSW AZ31 butt joint. Only the better quality butt joints are reported here. Cross section and upper surface macrostructure inspections reports are included

Specimen designation	ω/υ (rev mm^{-1})	Cross section	Upper surface
1000/50	20	Inner porosity detected at the advancing side in few specimens	Rough seam
1000/100	10	Inner porosity detected at the advancing side in all specimens	Slightly rough seam
1300/100	13	Inner porosity detected at the advancing side in all specimens	Slightly rough seam
1500/20	75	Inner porosity detected only at the advancing side in one specimen	Slightly rough seam
1500/50	30	Inner porosity detected at the advancing side in all specimens	Rough seam
2000/20	100	Inner porosity detected only at the advancing side in one specimen	Smooth seam
2000/50	40	Inner porosity detected only at the advancing side in one specimen	Rough seam

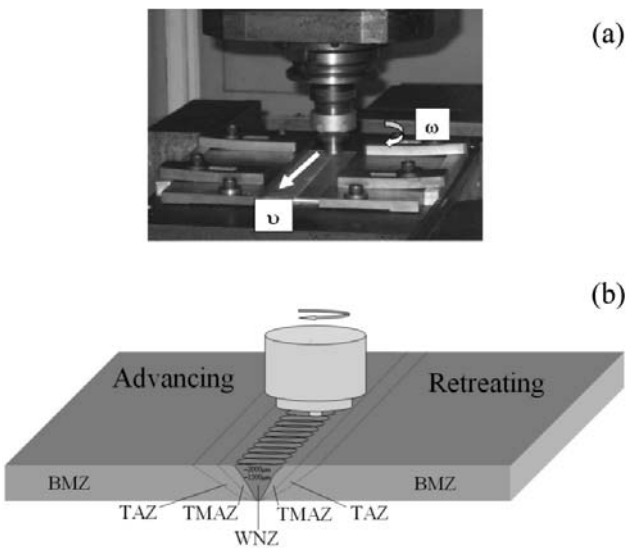

Fig. 1. a) The FSW process and system used in this study, probe revolution rate, ω, and its traverse velocity, υ, are indicated; b) scheme of the FSW macrostructure features of the AZ31B-H24 butt joint. The WNZ width is also reported.

dwelling time. Measurements were carried out on polished surfaces. Multiple measurements were taken through the mid-thickness of the sample cross section, and at the upper and lower surfaces, stretching from one base material, into the advancing half of the joint, through the transition and weld regions, and then into the other side, the retreating half of the joint. A minimum of 40 microhardness readings were taken along the thickness and along the upper and lower surfaces of the welded sample.

The nanoindenter Hysitron® UBI-1 was used for the nanohardness and reduced Young's modulus measurements. The nanoindenter was equipped with a Berkovich diamond tip calibrated in a fuse quartz plate. A trapezoidal load-unload function of 5-10-5 s with a peak load of 5000 μN was set for all the measurements. The Oliver and Pharr method was used for the analysis of all the load-unload displacement curves [29–31].

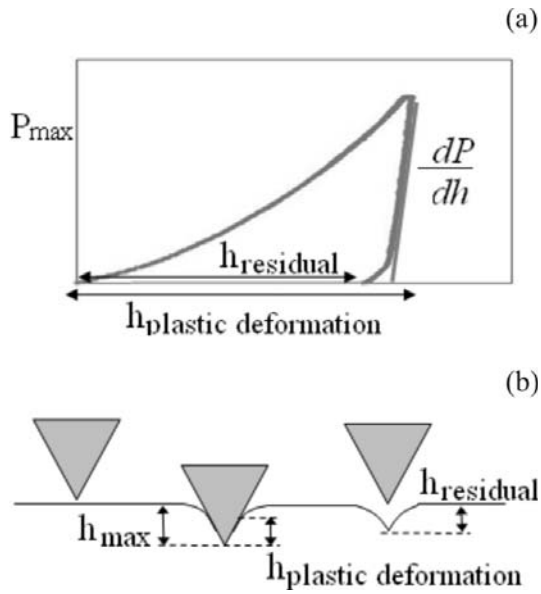

Fig. 2. a) Typical nanoindentation load-unload displacement curve, dP/dh, is the unload contact stiffness of the material; b) scheme of the indentation process for the evaluation of the nanohardness. The contact projective area, A, is a function of the plastic component of the penetration depth, $h_{\text{plastic deformation}}$.

The typical load-unload displacement curve is shown in Fig. 2a. One of the two major mechanical properties obtained is the hardness (nano-scale level):

$$H = P_{\max}/A, \tag{1}$$

where $P_{\max}$ is the peak load and A is the projection of the contact area at the load peak. Another important mechanical parameter is the reduced Young's modulus, E_{r} (which is a local evaluation of the material's Young's modulus):

$$E_{\mathrm{r}} = \frac{\sqrt{\pi}}{2}\frac{\mathrm{d}P}{\mathrm{d}h}\frac{1}{\sqrt{A}}, \tag{2a}$$

where dP/dh is the unloaded contact stiffness of the material (Fig. 2a).

Indeed, the reduced Young's modulus, E_r, is a measure of the elastic response of both tip, E_i, and material, E_c, in the load step:

$$\frac{1}{E_r} = \frac{(1-\nu_c)^2}{E_c} + \frac{(1-\nu_i)^2}{E_i}, \qquad (2b)$$

where ν is the Poisson's coefficient (which is 0.04 for the Berkovich tip used in this work), and E_i = 1171 GPa. The Berkovich tip has a pyramidal geometry with a triangular base. Thus, the relationship between the area, A, and the indentation depth, h_p, is: $A = 3\sqrt{3}h_p^2\tan^2(65.3) = 24.5h_p^2$ [31]. Substituting E_r in Eq. (2b) into Eq. (2a) and writing A in terms of h_p, the material reduced Young's modulus, E_c, is expressed as a function of the unloading curve slope, dP/dh (Eq. (2c)):

$$E_c = \frac{E_i(1-\nu_c)^2}{E_i-(1-\nu_i)^2}\frac{\sqrt{\pi}}{2}\frac{1}{24.5h_p^2}\frac{dP}{dh}. \qquad (2c)$$

Therefore, the material elastic modulus, E_c, can be determined by measuring the slope dP/dh at the unload curve, and knowing the Poisson's ratio of the material, ν_c, and the penetration depth of the tip at the peak load.

The penetration depth involves the plastic response of the material, and it will be at a depth well deeper than the residual print the tip will leave upon unloading (Fig. 2b).

The difference between the maximum depth, h_p, and the residual depth, h_{res}, rises with the material ductility. This is the key aspect that differentiates the nanohardness measurements from the more conventional Vickers microhardness, where the tip print is measured to obtain the hardness reading.

The exact estimation of the tip radius and curvature is of primary importance for the nanoindentation measurements. Routinely preliminary calibration procedures have to be run in order to calculate the tip radius and correct Eq. (2c) with a term called compliance (the reciprocal of the toughness):

$$E_c = \frac{E_i(1-\nu_c)^2}{E_i-(1-\nu_i)^2}\frac{\sqrt{\pi}}{2}\frac{1}{24.5h_p^2}\frac{dP}{dh} + C_i. \qquad (2d)$$

The contact area, A, is thus a function of the penetration depth, h_p, and this function can be calculated by interpolation, using Eq. (3) [32]:

$$A(h_p) = 24.5h_p^2 + c_1h_p + c_2h_p^{1/2} + c_3h_p^{1/4} + \\ + c_4h_p^{1/8} + \cdots + c_8h_p^{1/128}. \qquad (3)$$

Nanohardness and reduced Young's modulus were measured along the cross section and at the upper and lower surfaces of the FSW plate. The nanoindentation measurements started from the parent material zone (PMZ) through the heat affected zone (HAZ), thermo-mechanically affected zone (TMAZ), in the advancing half of the joint, and then to the nugget welded zone (NWZ), HAZ, TMAZ, and the PMZ, in the retreating half of the joint. Nanoindentations were placed each 330 nm, along lines parallel to the FSW joint profile.

3. Results and discussion

3.1. FSW process optimization

Figure 3 shows the macro images of the upper surfaces of the FSW butt joint at different FSW conditions in terms of probe revolution rate, ω, and traversing velocity, v. ω ranged from 1000 to 2000 rpm, the traversing velocity, v, ranged from 50 to 300 mm min^{-1}. It can be clearly seen that in all cases, for a given ω, the seam becomes wide and uniform as v decreases. The influence of v is mostly recognizable at ω = 1000 rpm, namely, tunnelling was detected at v = 200 and 300 mm min^{-1} in the advancing side. At ω = 1000 rpm and v = 100 mm min^{-1} flashes appear in the advancing side of the joint.

The ω dependence of v can be explained on the basis of heat input, namely, lower ω/v ratio means higher heat input and hence wider seam as also claimed by Gharacheh et al. [33]. For ω = 1000 rpm and v = 50 mm min^{-1} (ω/v = 20 rev mm^{-1}) a uniform and smooth seam was obtained, higher values of v = 100 mm min^{-1} (ω/v = 10 rev mm^{-1}) yielded a flash. Higher values of v = 200 mm min^{-1} and 300 mm min^{-1} (ω/v = 5 rev mm^{-1} and 3.33 rev mm^{-1}, respectively) yielded tunnelling at the advancing side of the weld. As for ω = 1300 rpm, an acceptable seam quality was obtained for ω/v = 26 rev mm^{-1} while flash appeared at ω/v = 13 rev mm^{-1}, 6.5 rev mm^{-1} and 4.33 rev mm^{-1}. For ω = 1300 rpm a uniform seam was obtained at ω/v = 75 rev mm^{-1} and some evidence of flash at ω/v = 50 rev mm^{-1}. In the case of ω = 2000 rpm a uniform seam was obtained for ω/v = 100 rev mm^{-1} and some evidence of flash at ω/v = 40 rev mm^{-1}. This result seems to contradict the findings of Commin et al. [34] who claimed that for 2 mm thick AZ31B-O plates a smooth seam was obtained when ω/v was decreased from 4 rev mm^{-1} to 1.6 rev mm^{-1}, while in the case of ω/v = 4 rev mm^{-1} a thick flash was produced.

Lowering the ω/v ratio has also a good influence as it results in a defect free weld, this is in line with the analysis of Zhang et al. [23] who studied the FSW of 5 mm thick AZ31 plates. The porosity was found to concentrate at the advancing side and this can be explained considering that the combined revolution of the probe and its linear traversing into the welding

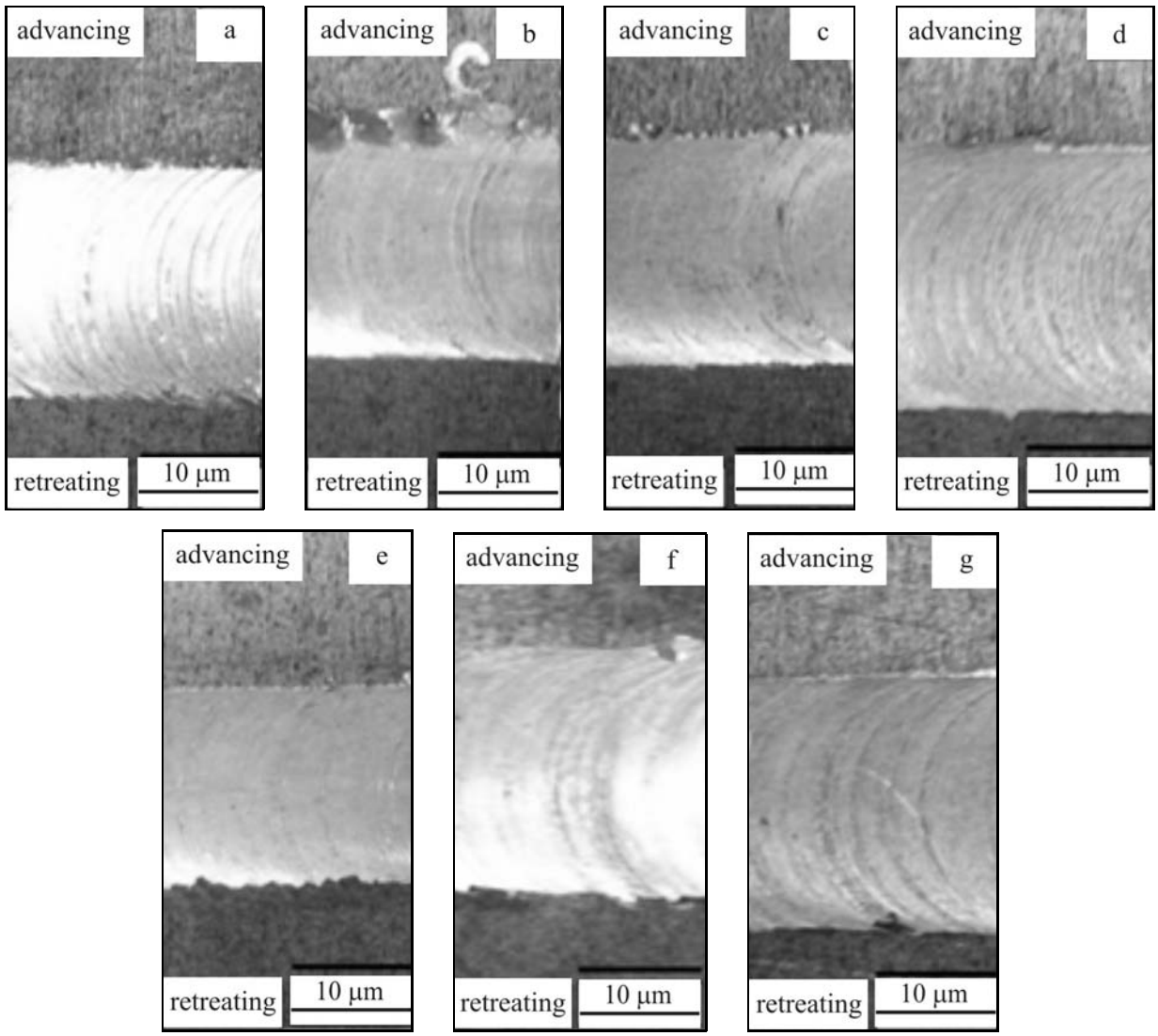

Fig. 3. Macrostructures of the FSW AZ31B-H24 butt joint as a function of the probe revolution rate, ω, and its traverse velocity, υ: a) $\omega/\upsilon = 1000/50$ rev mm^{-1}; b) $\omega/\upsilon = 1000/100$ rev mm^{-1}; c) $\omega/\upsilon = 1300/100$ rev mm^{-1}; d) $\omega/\upsilon = 1500/20$ rev mm^{-1}; e) $\omega/\upsilon = 1500/50$ rev mm^{-1}; f) $\omega/\upsilon = 200/500$ rev mm^{-1}; g) $\omega/\upsilon = 2000/20$ rev mm^{-1}.

plates transfers material from the advancing side to the retreating side [35]. Higher porosity was observed by both metallographic examination and radiographic inspections at the first third of the seam, this can be attributed to the heating of the welded part during process. It may be assumed that the required temperature is not achieved immediately after having put into contact the rotating probe and the two welding plates.

Pareek et al. [36] and Park et al. [37, 38], studying an AZ31 alloy, suggested that the strain rate in the nugget was largely controlled by the travel speed. When the traversing speed and the tool revolution rate are not effective enough to stir the plasticized material in front of the probe and to completely fill the rear of the trailing edge, pores can be formed. If the stirring action is strong enough, more mechanical bonding will be established. If the entrapped oxide films are fragmented, the oxides will become particles and will be dispersed in the stir zone, leading to the formation of solid inclusions. Good bonding can be reached at lower heat input (i.e. lower welding speed or higher tool revolution rate), resulting in the transformation of the continuous oxides into dispersed particles. At high welding speed, low heat input may cause lack of bonding and the formation of kissing bond defects. On the other hand at low welding speed, crack-like defects are most probably due to the lack of bonding or loose structure caused by inadequate material flow and mixing [39]. Notches formation might be related to the upward movement of the material in the stir zone. Zhang et al. [40] reported a virtually perfect butt joint with no evidence of defects or pores using a welding speed of 40 mm min^{-1}. Traces of pores were produced when

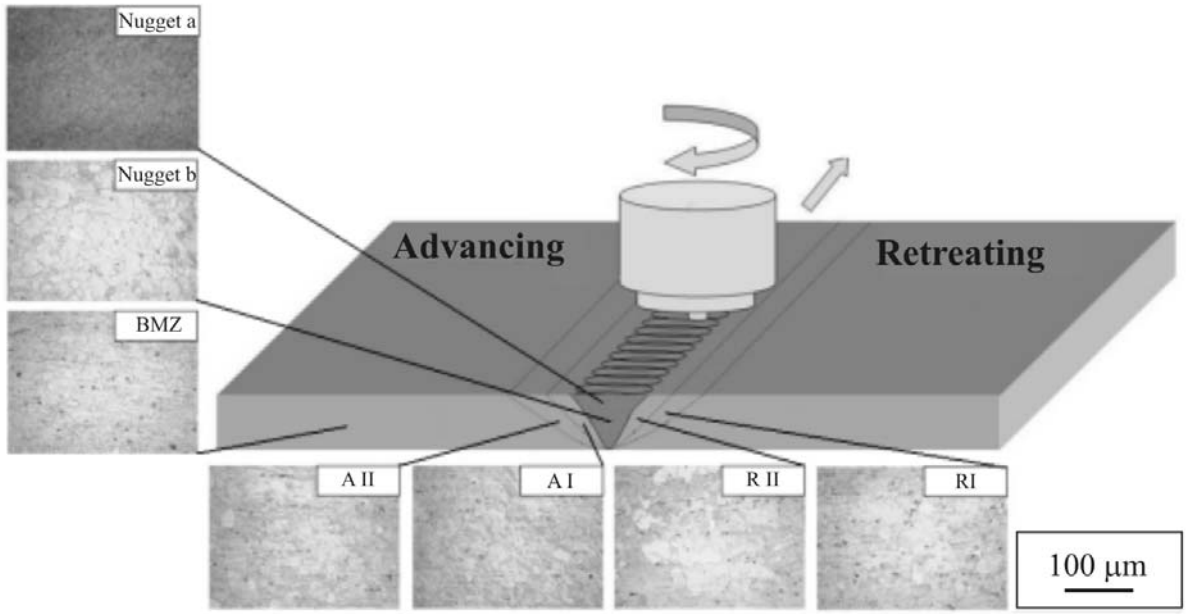

Fig. 4. Microstructures of the different FSW zones: BMZ, HAZ, TMAZ in the advancing side, WNZ, TMAZ, and HAZ in the retreating side of the cross section. A representative OM of the WNZ at the upper surface is also reported.

the welding speed reached 200 mm min^{-1}.

On the basis of the obtained results, radiographic inspections were carried out only on the 1500/20 and 2000/20 ω/υ specimens (namely, ω/υ = 75 and 100 rev mm^{-1}, respectively). The results of the radiographic inspections showed that the ω/υ = 1500/20 rev mm^{-1} butt joint contained inner porosity and/or cracks along about half of its length, while virtually 90 % of the ω/υ = 2000/20 rev mm^{-1} FSW joints were found to be sound. Thereafter, the ω/υ = 2000/20 (100 rev mm^{-1}) FSW condition was the one selected for the microstructure and the nanoindentation studies.

3.2. Microstructure inspections

Compared to the traditional welding methods, the microstructure of FSW joint exhibits unique characteristics. The schematic diagram of the typical zones in the cross section of the FSW joint is shown in Fig. 1b. The FSW joint can be divided into four zones: the base metal zone (BMZ), the heat-affected zone (HAZ), the thermo-mechanical affected zone (TMAZ), and the weld nugget zone (WNZ). The different zones are actually to be considered six as the HAZ and TMAZ in the advancing side usually show a different mechanical and microstructure morphology compared to the retreating side. The width of the WNZ, at the upper surface, at mid-thickness of the cross section, and at the bottom surface were ∼ 2000, ∼ 1500, and ∼ 750 μm, respectively. TMAZ and HAZ in the advancing and retreating side of the joint were not symmetrical, being wider in the retreating side. The microstructure of the BMZ (Fig. 4) showed equiaxed grains with mean size of 10 ± 2 μm. The HAZ showed larger and still equiaxed grains with a mean size of 21 ± 3 μm. In the TMAZ coexisted slightly elongated grains with equiaxed ones. Grains were crossed by shear bands induced by the stirring of the traversing and rotating probe. Mean grain size (24 ± 4 μm) in the TMAZ was slightly larger than in the HAZ. The WNZ grain sizes were quite similar to the ones in TMAZ and HAZ, and were 20 ± 4 μm.

Thus, the HAZ experienced a partial recrystallization. The recrystallization temperature for the alloy is approximately 205 ℃ [33]. Thus, during FSW, the temperature in part of the HAZ is likely to have been well above this value. This is confirmed by some large grains observed in the HAZ (Fig. 4. – A_1 and R_1) due to growth after recrystallization. The material in the HAZ was neither stirred by the probe nor rubbed by the shoulder, and it experienced a heating process only due to the heat conduction. Therefore, the crystal grains in the HAZ grew up and became coarser than those in the BMZ. TMAZ (Fig. 4 – AII and RII) was mainly composed of equiaxed grains indicating that recrystallization had already taken place. The metal in the TMAZ is located at the edge of the tool. The plastic flow and deformation of grains occurred because of the revolution and stir of the tool. Most of the grains were stretched along the direction of the moving tool. Most of the microstructures in the TMAZ experienced the dynamic recovery (DRV) and dynamic recrystallization (DRX) process, and some grains even grew up. Similar results were reported by Cao and Jahazi [41] and Afrin et al. [20].

The equiaxed grains in the WNZ (Fig. 4 – Nugget a and Nugget b) are formed by DRX. In the present case, the recrystallized grains also experienced a grain growth. Other authors, Esparza et al. [8] and Park et al. [26, 37], in other studies and for similar magnesium alloys, reported different results. Anyhow, the probe traverse velocity and revolution rate were different, as well as the initial condition of the butt welded alloys. As a matter of fact, the strain rate in the WNZ is mainly controlled by the welding speed, i.e. higher welding speed will lead to higher strain rate [33]. Clearly, the grain growth or refinement depends on the microstructure of the base metal and the kinetics of recrystallization and grain growth.

The microstructure inspections at the upper and lower surfaces of the AZ31 FSW butt joint showed some significant differences. At the upper surface grains in the BMZ were equiaxed and homogeneous with a mean size of 19 ± 1 μm. The TMAZ experienced a DRX and traces of stirring are visible. The grains grew to more than double the size of the BMZ in the WNZ and TMAZ. At the bottom surface the HAZ and TMAZ zones were more confused and their width was very small. A non-homogeneous grain structure characterized the whole profile of the bottom surface that showed large grains and smaller ones from the BMZ in the advancing side to the opposite BMZ in the retreating side of the joint. In the WNZ slightly larger grains were observed on the upper surface compared to the bottom surface. The formation of larger grains in the stir zone was also reported by Lim et al. [24] and Pareek et al. [36] for an AZ31-H24 alloy. Similarly, Chang et al. [17] observed a smaller grain size at the bottom than at the upper surface of FSW AZ31 magnesium alloy. Therefore, the frictional heat generated by the rubbing of the tool shoulder and the mechanical stirring of the materials by the tool probe provided the driving force for the DRX of the materials in the WNZ. This enabled the severe plastic deformation in the weld zone to be accommodated by the flow of the material in the solid state. Hence, DRX facilitates the solid-state flow during FSW.

3.3. Nanoindentation and microhardness measurements

Figure 5 shows the nanohardness and microhardness profiles along the mid-thickness cross section and along the upper and bottom surfaces. In the cross section the WNZ showed lower microhardness compared to the BMZ. This is most likely to be attributed to larger mean grain size of the WNZ compared to the grain size of the parent material, in agreement with some previous results where larger grains in the WNZ, compared to the BMZ, were also reported [42]. A quite similar microhardness profile was reported by Afrin and co-workers in [20]. Others [17, 18] reported only

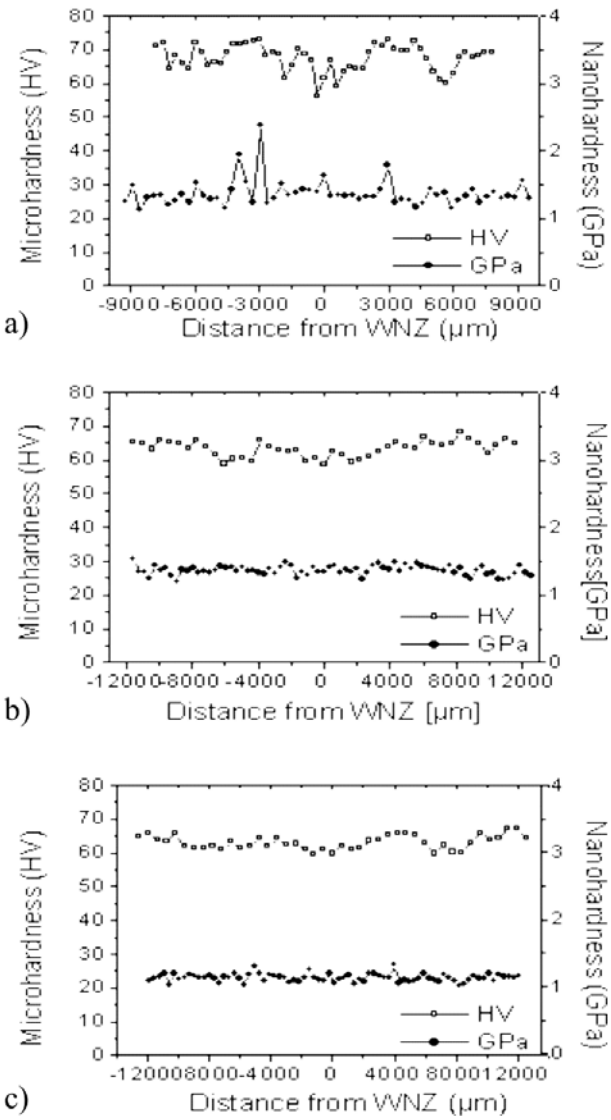

Fig. 5. Nanohardness and microhardness profiles along a) the mid-thickness cross section, b) the upper surface, c) the bottom surface.

a weak influence of grain size on hardness changes in FSW AZ31B Mg alloy. On the other hand, Nagasawa et al. [43] found smaller grain size in the WNZ of a hot rolled AZ31B plate with insignificant difference in the hardness between the WNZ and the BMZ.

Microhardness resulted higher in the upper surface than at the lower surface of the welded plate. The observed wavy trend of the microhardness profile across the different regions of the FSW AZ31 plate was also reported by Dobriyal et al. [44].

Due to the strong friction of the shoulder to the material, the distribution of the stir and friction heat is non-uniform, and there exists a negative temperature gradient from the upper to the lower surface. Thus, the grain size in the upper surface of the weld is larger than that in the lower, resulting in a microhardness increase.

Table 2. Mean nanohardness at reduced Young's modulus in the upper, mid-thickness cross section, and the lower surface of the AZ31B-H24 FSW butt joint

	Nanohardness (GPa)	Reduced Young's modulus (GPa)
Cross section	1.2 ± 0.2	53 ± 3
Upper surface	1.15 ± 0.05	43 ± 2
Lower surface	1.35 ± 0.05	47 ± 2

The nanohardness profile, recorded along the upper and along the bottom surfaces of the butt joint, showed no significant difference of hardness between the WNZ and the BMZ. On the other hand, along the cross section, a peak was observed in the advancing and retreating side corresponding to the interface between TMAZ and HAZ. Both aspects are related to the microstructure features to which the nanoindentation is sensitive. According to Dix and Gao [45], the nanohardness measurements are strongly related to the statistically stored and geometrically necessary dislocation densities. The former is generated by shearing and plastic deformation of the crystalline metallic material; the latter is essentially a density of dislocations belonging to the high-angle and low-angle boundaries (i.e. grain and sub-grain boundaries). Since the grain size of the TMAZ and WNZ was found to be essentially alike, the geometrically necessary dislocation density will not change significantly. On the other hand, the larger recrystallized grains in the WNZ, compared to the BMZ, will reduce the geometrically necessary dislocation density in the WNZ compared to the BMZ. The statistically stored dislocation density will rise chiefly in the TMAZ, here shear deformation occurred and was detected, but it will also rise, even if with a lower extent, in the WNZ. Therefore, the peak of nanohardness at the edge of the TMAZ (corresponding to the FSW probe border) is due to the rise in the density of the two types of dislocations. The similar nanohardness between the WNZ and the BMZ is due to a combination of the two dislocation components. In the WNZ, the statistically stored dislocation density is larger than that in the BMZ (plastic deformation during FSW), while the geometrically necessary one is larger in the BMZ (larger grains in the WNZ).

The mean nanohardness from the upper to the lower surface decreased from 1.35 ± 0.5 to 1.15 ± 0.5 GPa (Table 2), while the microhardness did not show any significant change. This is clearly due to a profound different meaning of the two techniques. The nanoindentation showed a much lower dependence on Hall-Petch relationship compared to the microhardness, which is known to be strongly related to it [20, 41]. This is because nanoindentation is a nanoscale hardness measurement, that is, it is strongly bound to tangle dislocations, to the geometrical and the necessary dislocations existing beneath the interaction volume, and not simply to the alloy grain size.

The reduced Young's modulus values at the different characteristic regions of the FSW butt joint did not show any significant variation. The reduced Young's modulus values obtained at the mid-thickness of the cross section, and upper and lower surfaces are reported in Table 2. The measured reduced Young's modulus is equal to the magnesium alloy Young's modulus (45 GPa), this value being essentially constant between the upper and lower surface. A slightly larger Young's modulus was obtained along the cross section and this is likely to be attributed to the stirring process during FSW which is more evident at the TD-ND plane. As a matter of fact, the stirred grains and cells develop an increased rigidity and a slight hardness increment, as also shown in Fig. 5. This is generally due to the complex grain and cell boundary geometrical deformation induced by the rotating tool, which promotes a lateral size reduction and longitudinal curly-like elongation of the grains and cells that eventually generate high aspect-ratio structures.

4. Conclusions

An AZ31B-H24 magnesium alloy was FSW using different probe traverse speed and revolution rates. The quality of the FSW butt joint was detected by macrostructure observations and by radiographic inspections. It was found that the probe traverse velocity of 20 mm min^{-1} and revolution rate of 2000 rpm were the FSW optimization condition, since a sound and pore-free butt joint was produced.

Optical microstructure observations of the FSW joint showed that the grain size in the WNZ was larger than the one in the BMZ. The WNZ and the TMAZ experienced a DRX and eventually a grain coarsening. TMAZ was characterized by a diffuse stirring and shearing of the grains. HAZ had grain size larger than the BMZ but finer than the ones in the TMAZ and WNZ. The width of the TMAZ and HAZ in the retreating side was wider than that in the advancing side.

The lowest microhardness was in the WNZ, due to a coarsening of the recrystallized grains. The highest values were at the TMAZ in both advancing and retreating side of the AZ31 FSW butt joint.

Nanohardness showed no significant difference

between the mean values in the WNZ and the BMZ. Peaks were found at the TMZ/HAZ interface and the maximum peak was in the advancing side. The differences between nanohardness and microhardness are to be ascribed to the microstructure sensitiveness of the two methods. The microhardness is strongly related to Hall-Petch, while the nanohardness is strongly related to the statistically stored and geometrically necessary dislocation densities within the different zones of the FSW butt joint.

Acknowledgements

Authors (M. Cabibbo and P. Ricci) wish to thank Mr. D. Ciccarelli for the OM specimens preparation. This research project is partly financed by Ort Braude College of Engineering, Israel. Thanks are due to Dr. A. Katz-Demyanetz, Mr. H. Shalem and Mr. E. Resel.

References

[1] MORDIKE, B. L.—EBERT, T.: Mater. Sci. Eng. A, *302*, 2001, p. 37. doi:10.1016/S0921-5093(00)01351-4
[2] AGHION, E.—BRONFIN, B.: Material Science Forum, *350*, 2000, p. 19. doi:10.4028/www.scientific.net/MSF.350-351.19
[3] POLMEAR, I. J.: Materials Science and Technology, 10, 1994, p. 1.
[4] NIEH, T. G.—WADSWORTH, J.: Scripta Mater., *32*, 1995, p. 1133. doi:10.1016/0956-716X(94)00016-B
[5] XIE, G. M.—MA, Z. Y.—GENG, L.—CHEN, R. S.: Materials Science and Eng. A, *471*, 2007, p. 63. doi:10.1016/j.msea.2007.03.041
[6] THOMAS, W. M.: International Patent Application No. PCT/GB92/02203; GB Patent Application No. 9125978.8, 6, 1991; U.S. Patent No. 5,460,317.
[7] ESPARZA, J. A.—DAVIS, W. C.—MURR, L. E.: J. Mater. Sci., *38*, 2003, p. 941. doi:10.1023/A:1022321107957
[8] ESPARZA, J. A.—DAVIS, W. C.—TRILLO, E. A.—MURR, L. E.: J. Mater. Sci. Lett., *21*, 2002, p. 917. doi:10.1023/A:1016061303955
[9] JOHNSON, R.: Mater. Sci. Forum, *419–422*, 2003, p. 365. doi:10.4028/www.scientific.net/MSF.419-422.365
[10] KIM, T.—KIM, J.—HASEGAWA, Y.—SUGA, Y.: In: Proceedings Third Intern. Symposium on Designing, Processing and Properties of Advanced Engineering Materials. Jeju Island, South Korea 2003, p. 417.
[11] ZENG, R. C.—KE, W.—XU, Y. B.—HAN, E. H.—ZHU, Z. Y.: Acta Metall. Sinica, *37*, 2001, p. 673.
[12] ZHANG, D.—SUZUKI, M.—MARUYAMA, K.: Scripta Mater., *52*, 2005, p. 899. doi:10.1016/j.scriptamat.2005.01.003
[13] NIEH, T. G.—WADSWORTH, J.: Scripta Mater., *32*, 1995, p. 1133. doi:10.1016/0956-716X(94)00016-B
[14] WATANABE, H.—MUKAI, T.—MABUCHI, M.—HIGASHI, K.: Scripta Mater., *41*, 1999, p. 209. doi:10.1016/S1359-6462(99)00155-4
[15] Del VALLE, J. A.—PEREZ-PRADO, M. T.—RUANO, R. O.: Mater. Sci. Eng., *355A*, 2003, p. 68.
[16] MISHRA, R. S.—MA, Z. Y.: Mater. Sci. Eng. R, *50*, 2005, p. 1. doi:10.1016/j.mser.2005.07.001
[17] CHANG, C. I.—LEE, C. J.—HUANG, J. C.: Scripta Mater., *51*, 2004, p. 509. doi:10.1016/j.scriptamat.2004.05.043
[18] WANG, Y. N.—CHANG, C. I.—LEE, C. J.—LIN, H. K.—HUANG, J. C.: Scripta Mater., *55*, 2006, p. 637. doi:10.1016/j.scriptamat.2006.06.005
[19] SOMASEKHARAN, A. C.—MURR, L. E.: Mater. Charact., *54*, 2004, p. 49. doi:10.1016/j.matchar.2004.03.005
[20] AFRIN, N.—CHEN, D. L.—CAO, X.—JAHAZI, M.: Mater. Sci. Eng. A, *472*, 2008, p. 179. doi:10.1016/j.msea.2007.03.018
[21] SATO, Y. S.—PARK, S. H. C.—MATUSUNAGA, A.—HONDA, A.—KOKAWA, H.: J. Mater. Sci., *40*, 2005, p. 637. doi:10.1007/s10853-005-6301-1
[22] FENG, A. H.—MA, Z. Y.: Scripta Mater., *56*, 2007, p. 397. doi:10.1016/j.scriptamat.2006.10.035
[23] ZHANG, H.—LIN, S. B.—WU, L.—FENG, J. C.—MA, S. L.: Mater. Des., *27*, 2006, p. 805. doi:10.1016/j.matdes.2005.01.016
[24] LIM, S.—KIM, S.—LEE, C. G.—YIM, C. D.—KIM, S. J.: Metall. Mater. Trans. A, *36*, 2005, p. 1609. doi:10.1007/s11661-005-0252-7
[25] LEE, W. B.—KIM, J. W.—YEON, Y. M.—JUNG, S. B.: Mater. Trans., *44*, 2003, p. 917. doi:10.2320/matertrans.44.917
[26] PARK, S. H. C.—SATO, Y. S.—KOKAWA, H.: J. Mater. Sci., *38*, 2003, p. 4379. doi:10.1023/A:1026351619636
[27] MIRSHAMS, R. A.—PARAKALA, P.: Mater. Sci. Eng. A, *372*, 2004, p. 252. doi:10.1016/j.msea.2004.01.010
[28] PHARR, G. M.: Mater. Sci. Eng. A, *253*, 1998, p. 151. doi:10.1016/S0921-5093(98)00724-2
[29] OLIVER, W. C.—PHARR, G. M.: J. Mater. Res., *7*, 1992, p. 1564. doi:10.1557/JMR.1992.1564
[30] NIX, W. D.—GAO, H.: J. Mech. Phys. Solids, *46*, 1998, p. 411. doi:10.1016/S0022-5096(97)00086-0
[31] FISCHER-CRIPPS, A. C.: Vacuum, *58*, 2000, p. 569. doi:10.1016/S0042-207X(00)00377-8
[32] RO, Y. J.—BEGLEY, M. R.—GANGLOFF, R. P.—AGNEW, S. R.: Mater. Sci. Eng. A, *435–436*, 2006, p. 333. doi:10.1016/j.msea.2006.07.102
[33] GHARACHEH, A. M.—KOKABI, A. H.—DANESHI, G. H.—SHALCHI, B.—SARRAFI, R.: Int. Journal of Machine Tools & Manuf., *46*, 2006, p. 1983.
[34] COMMIN, L.—DUMONT, M.—MASSE, J. E.—BARRALLIER, L.: Acta Mater., *57*, 2009, p. 326. doi:10.1016/j.actamat.2008.09.011
[35] CABIBBO, M.—McQUEEN, H. J.—EVANGELISTA, E.—SPIGARELLI, S.—Di PAOLA, M.—FALCHERO, A.: Mater. Sci. Eng. A, *460–461*, 2007, p. 86. doi:10.1016/j.msea.2007.01.022
[36] PAREEK, M.—POLAR, A.—RUMICHE, F.—INDACOCHEA, J. E.: J. Mater. Eng. Perform., *16*, 2007, p. 655. doi:10.1007/s11665-007-9084-5
[37] PARK, S. H. C.—SATO, Y. S.—KOKAWA, H.: Metall. Mater. Trans. A, *34*, 2003, p. 987. doi:10.1007/s11661-003-0228-4

[38] PARK, S. H. C.—SATO, Y. S.—KOKAWA, H.: Scripta Mater., *49*, 2003, p. 161. doi:10.1016/S1359-6462(03)00210-0
[39] DARRAS, B. M.—KHARAISHEH, M. K.—ABU-FARHA, F. K.—OMAR, M. A.: J. Mater. Proc. Techn., *191*, 2007, p. 77. doi:10.1016/j.jmatprotec.2007.03.045
[40] ZHANG, H.—LIN, S. B.—WU, L.—FENG, J. C.: J. Aeronautic Mater., *24*, 2004, p. 6.
[41] CAO, X.—JAHAZI, M.: Mater. Des., *30*, 2009, p. 2033.
[42] WANG, X.—WANG, K.: Mater. Sci. Eng. A, *431*, 2006, p. 114.
[43] NAGASAWA, T.—OTSUKA, M.—YOKOTA, T.—UEKI, T: Magnesium Technology 2000, TMS, 2000, p. 383.
[44] DOBRIYAL, R. P.—DHINDAW, B. K.—MUTHU-KUMARAN, S.—MUKERJEE, S. K.: Mater. Sci. Eng. A, *477*, 2008, p. 243. doi:10.1016/j.msea.2007.06.028
[45] NIX, W. D.—GAO, H.: J. Mech. Phys. Solids, *46*, 1998, p. 411. doi:10.1016/S0022-5096(97)00086-0